ALOS-2 AUTONOMOUS ORBIT CONTROL - ONE-YEAR EXPERIENCE OF FLIGHT DYNAMICS OPERATION

Toru Yamamoto[1], Yoshihisa Arikawa[2], Yasushi Ueda[3], Hiroyuki Itoh[4], Yoshitaka Nishida[5], Hiroyoshi Tsuru[6], Shinichi Ukawa[7], and Masayuki Yamamoto[8]

[1][2][3][4]*Japan Aerospace Exploration Agency, Tsukuba, 305-8505, Japan, +81-50-3362-4356, yamamoto.toru@jaxa.jp*

[5][6][7]*Mitsubishi Electric Co., Ltd., Kamakura, 247-8520, Japan*

[8]*Mitsubishi Space Software Co., Ltd., Tsukuba, 305-0032, Japan*

Abstract: *ALOS-2, the Japanese state-of-the-art L-band SAR satellite, is designed to perform autonomous precise orbit control of Earth-referenced repeating orbits for effective repeat-pass SAR interferometry. The orbit control accuracy requirement is 500 m (95%) with respect to the reference trajectory. Since its activation in August 2014, it has been operated normally and contributed to ALOS-2 mission data quality improvement. This paper addresses not only evaluation results of the achieved control performance but also experiences during one-year operation of the ALOS-2 autonomous orbit control system.*

Keywords: *Autonomous Orbit Control, On-board Autonomy, Flight Dynamics Operation, Repeat-pass SAR Interferometry.*

Nomenclature

a	=	semi-major axis
$\boldsymbol{E}$	=	space error, $\boldsymbol{E} = (E_N, E_R)^T$
$\boldsymbol{e}$	=	eccentricity vector, $\boldsymbol{e} = (e_x, e_y)^T = (e\cos\omega, e\sin\omega)^T$
i	=	inclination
J_2	=	second zonal gravity harmonic of the Earth
k	=	serial number of checkpoints or integer number
L_s	=	Mean Local Time (MLT) of the descending node
M	=	mean anomaly
n	=	mean motion
R	=	disturbing function or equatorial radius
$\boldsymbol{r}$	=	position vector in WGS-84
T	=	nodal period
t	=	time
u	=	argument of latitude
v	=	velocity
x, y, z	=	position in WGS-84
$\boldsymbol{\alpha}$	=	orbital element vector, $\boldsymbol{\alpha} = \left(T, \bar{\boldsymbol{e}}^T, \bar{i}, \lambda\right)^T$
α	=	phase angle
γ	=	angle between the inertial and Earth-fixed velocity vectors
ε	=	error ratio, or mean obliquity of ecliptic
κ	=	ratio of mean anomaly n to nodal regression rate $\dot{\Omega}$
λ	=	longitude

μ	=	gravitational constant
Ω	=	right ascension of ascending node
ω	=	argument of perigee or angular velocity

Subscript

$cross$	=	cross-track direction
DN	=	descending node
E	=	east
e	=	Earth
HM	=	periodic perturbation with half-month period
I	=	epoch of next maneuver
j	=	pass number
LP	=	periodic perturbation with long period
l	=	local
m	=	maneuver number or Moon
max	=	maximum
$meas$	=	measurement
min	=	minimum
N	=	normal direction of Radial-Tangential-Normal frame
R	=	radial direction of Radial-Tangential-Normal frame
$radial$	=	radial direction
ref	=	reference orbit
S	=	secular perturbation
SL	=	secular and long period perturbations
s	=	Sun
T	=	tangential direction of Radial-Tangential-Normal frame
th	=	threshold
tg	=	target
W	=	west
0	=	epoch of computation
$\bar{}$	=	mean value

1. Introduction

Advanced Land Observing Satellite-2 (ALOS-2), which is a Japanese Earth observation satellite equipped with the state-of-the-art L-band SAR instrument, has an autonomous orbit control function for precisely keeping its trajectory within the 500-m-radius tube-shaped corridor defined in the Earth-fixed coordinate system. This autonomous orbit control feature of ALOS-2 has been in practical use since its activation in August 2014, and it has been a great help for precision maintenance of the orbitand efficient daily ground operations.

Some Earth observation satellites that carry synthetic aperture radar (SAR) instruments have more stringent requirements for precision orbit control of Earth-fixed repeating orbits than conventional

Earth observation satellites. This requirement arises from the geometric constraints for effective repeat-pass SAR interferometry. Tight maintenance of Earth-fixed repeating orbits ensures good coherence between repeat-pass SAR image pairs. For this purpose, the SAR satellite must fly within a tube-shaped corridor, the center of which is the Earth-fixed reference trajectory. The greater the orbit control accuracy requirement, the higher the frequency of orbital maneuvers required. In particular, the frequency significantly increases during the active solar period due to high atmospheric density. An orbit control operation, which comprises many tasks (orbit determination, maneuver planning, maneuver commanding and maneuver execution), imposes a considerable workload; therefore, frequent maneuvers become a burden in everyday ground operations. Autonomous orbit control can be a solution for this problem. The workload and the costs of orbit control operations can be reduced by sophisticated on-board software that can handle a series of necessary tasks in orbit control operations. Fully automatic decisions regarding maneuvers by on-board software, however, create a new problem when the autonomous orbit control approach is applied to practical Earth observation missions. The problem arises from unexpected timing conflicts between maneuver executions and mission observations. If the on-board software determines the time of a maneuver without considering mission observations, an automatic orbital maneuver may ruin important observation opportunities.The time of a maneuver should threfore be planned carefully so that the maneuver does not interfere with planned mission observations.

With the above issues in mind, the authors applied the autonomous orbit control approach to the ALOS-2 mission. This applied method can achieve autonomous operations of orbit determination, maneuver prediction, maneuver planning, and maneuver executions. Both in-plane and out-of-plane maneuvers are planned and executed autonomously so that the satellite flies within a tube-shaped corridor, the center of which is the Earth-fixed reference trajectory. The maneuver planning algorithms can place the time of a maneuver so that it does not spoil the observations by using the proposed “maneuver slot” concept.

ALOS-2 was successfully launched on May 24th 2014. Its orbit is a 628-km sun-synchronous repeating orbit with a 14-day repeat cycle. The orbit control requirement for the radius of the tube-shaped corridor is 500 m (95%).

The applied method has been demonstrated in practical use since its activation in August 2014. This is the world’s first attempt to apply autonomous precision orbit control within a tube-shaped corridor for a regular-basis operation of an Earth observation satellite. In this paper, the practical aspects of the ALOS-2 flight dynamics operations are the primary subject of discussion. Not only the achieved control performance but also the lessons learned from one year of actual flight dynamics operations, such as reactions to solar activity change and debris avoidance maneuvers, are reported.

2. ALOS-2 Mission and Spacecraft

ALOS-2 has two mission objectives [1]. The first is to contribute to the disaster management activities of the central and local governments in Japan and foreign countries by observing disaster-stricken areas widely and in detail, regardless of the time (day or night) or the weather, and by establishing a system to quickly obtain, process, and share observation data. The second objective is to promote data utilization in various fields with constant observation data to meet user needs.

This includes 1) continuous monitoring of social infrastructures such as roads, railroad tracks, and bridges, 2) understanding agricultural conditions, and 3) global monitoring of tropical rain forests to identify carbon sinks. ALOS-2 carries the state-of-the-art L-band SAR instrument PALSAR-2, which enables the capture of wide and high-resolution observation data of the Earth's surface.

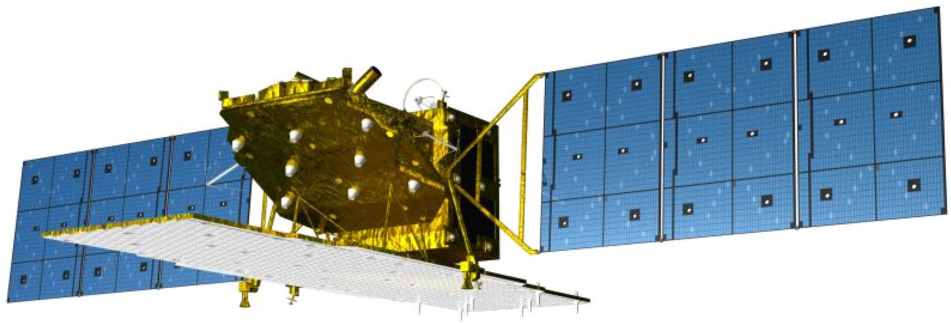

Figure 1. ALOS-2 in-orbit configuration.

The key parameters of ALOS-2 related to autonomous orbit control are shown in Table 1. Its orbit is a 628-km sun-synchronous repeating orbit with a 14-day repeat cycle. The orbit control requirement for the radius of the tube-shaped control window is 500 m (95%). The on-board GPS receiver provides accurate real-time orbit information, whereas the fully redundant four 4 N hydrazine thrusters are located on one side of the spacecraft and its thrust vectors are along the anti-velocity direction when the satellite is in the nominal local-vertical local-horizontal (LVLH) attitude. This means that the satellite must perform 180° yaw-around attitude maneuvers for a deceleration maneuver.

3. Definition of Control Problem

3.1. ALOS-2 Orbit Control Requirement

SAR repeat-pass interferometry imposes tight restrictions on the orbit control, requiring a tube-shaped control window with a radius ranging from 50 to 1000 m. SAR interferometry is a technique that exploits pairs of SAR data acquired by two observations over the same ground target and extracts the phase difference of the data pair to yield the heights of the observed terrain. SAR interferometry can be accomplished with formation flying of two SAR satellites like TanDEM-X/TerraSAR-X [2] or by repeat-pass recurrent observations of a single SAR satellite [3]. Figure 2 shows the geometry of the repeat-pass SAR interferometry.

The perpendicular baseline is the spatial distance between the first and second observations and is measured perpendicular to the viewing direction. This perpendicular baseline must be short enough to achieve sufficient coherence in interferometry [4]; therefore, an SAR satellite must fly along the same reference trajectory for each recurrent cycle. Accordingly, the repeating Earth-fixed reference trajectory is defined for a repeat cycle and a SAR satellite must fly within the tube-shaped control window, which centers on the reference trajectory. The orbit control margin can be imagined as a tube defined around the spacecraft reference trajectory with a certain radius.

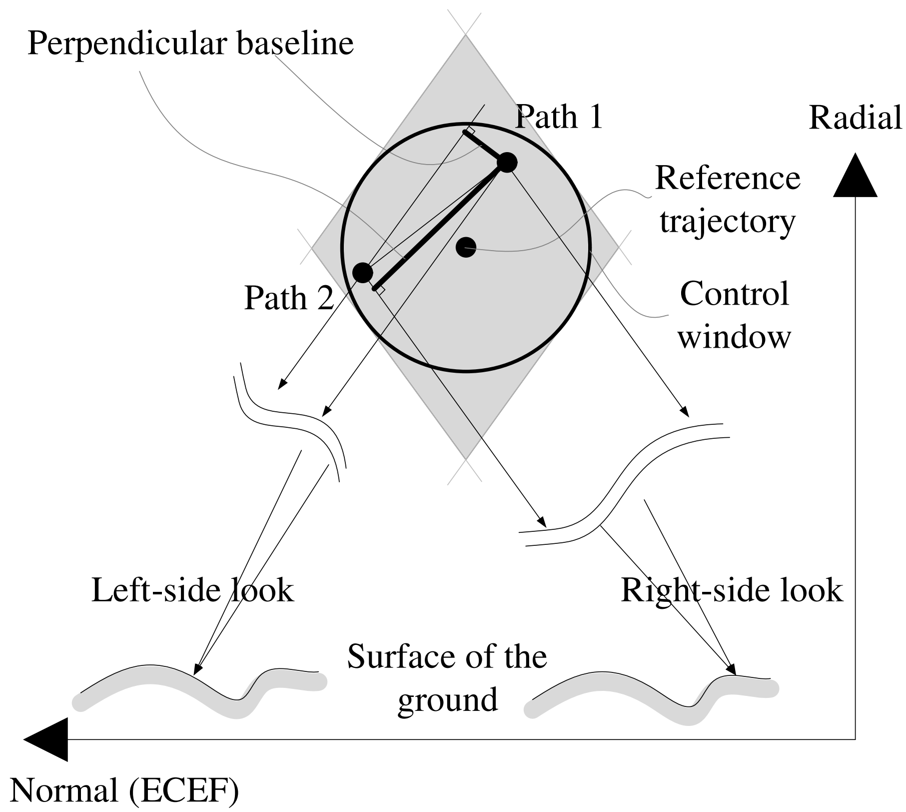

Figure 2. Geometry of repeat-pass SAR interferometry.

Table 1. Key parameters of ALOS-2 in terms of orbit control

Parameter	Value
Orbit type	Sun-synchronous repeating orbit
Altitude	628 km
Repeat cycle	14 days, 207 orbital revolutions
Mean Local Time (MLT)	12:00 $\pm$ 15 min (at the descending node)
Satellite size	Approx. 9.9 $\times$ 16.5 $\times$ 3.7 m^3
Satellite mass	Approx. 2 tons
Orbit control requirement	Tube-shaped control window less than 500 m (95%)
On-board GPS navigation	Position 13 m max, 4.2 m typ. (95%) Velocity 0.06 m/s max, 0.013 m/s typ. (95%)
Thrusters	Full-redundant four 4 N hydrazine thrusters equipped along anti-velocity direction

To characterize and evaluate the control errors of the SAR orbital tube control problem rigorously, a variable so-called space error $\boldsymbol{E}$ is defined and introduced [5]. The definition of the space error is shown in Fig. 3. Both the reference trajectory and the actual trajectory of the spacecraft are osculating orbits expressed in the Earth-Centered Earth-Fixed (ECEF) frame. In other words they are ground-tracks projected at the altitude of the spacecraft. Equally spaced check-points are defined on the reference trajectory. At each check-point, the evaluation plane formed by the radial and normal (ECEF) axes is defined. The space error $\boldsymbol{E}_k$ for the check-point k is the vector difference on the evaluation plane, from the piercing point of the reference trajectory to that of the actual trajectory. The space error $\boldsymbol{E}$ comprises its normal (ECEF) and radial components: $\boldsymbol{E} = (E_N, E_R)^T$. Due to the along-track displacement between the reference and actual trajectories, the space error should not be evaluated with positions at the same epoch (meaning the same absolute time). The position of the reference trajectory at the check-point k: $\boldsymbol{r}_{ref}(t_k)$ should be compared with the position of the actual spacecraft at the time when the actual trajectory arrives at the corresponding evaluation plane: $\boldsymbol{r}(t_k + \Delta t)$.

The orbit control requirement for the SAR spacecraft is to keep the space error $\boldsymbol{E}$ within a specified deadband at every checkpoint on the reference trajectory. For the ALOS-2 mission the space error should be less than 500 m over 95% of the time, which guarantees the proper perpendicular baseline length for the ALOS-2 repeat-pass SAR interferometry.

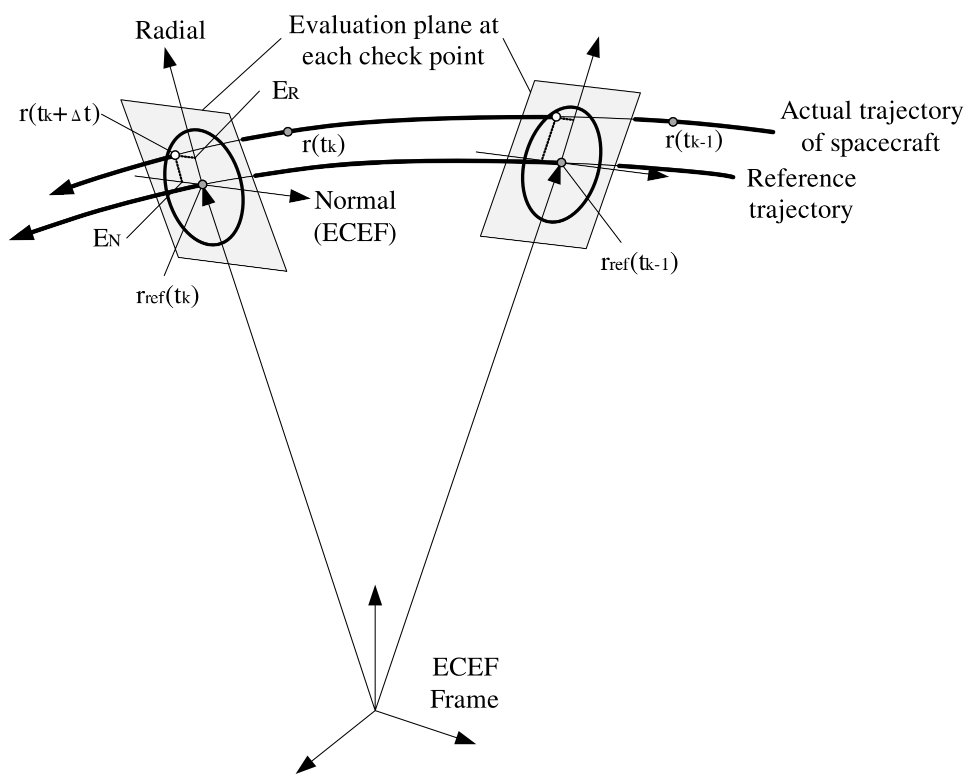

Figure 3. Definition of space error *E*.

3.2. Reference Trajectory Parametrization

The Earth-fixed reference trajectory, which is an osculating orbit for a repeat cycle, is the target of the autonomous orbit control. The repeat cycle of ALOS-2 is exactly 14 days, 207 orbital revolutions. Each revolution of a repeat cycle has a unique path number, which goes from 1 to 207 in chronological order. If the reference trajectory of each repeat cycle differs from the others, the difference directly contributes to an increase in the space error. Therefore, the reference trajectory should be identical for each repeat cycle throughout the mission life of a satellite. This means that any pair of reference trajectories in one orbital revolution with the same path number should be exactly identical to each other, regardless of the repeating cycles.

The requirements for the reference trajectory of the ALOS-2 mission is as follows:

- An approx. 628 km altitude
- An exact 14 days, 207 orbital revolutions repeat cycle
- A frozen orbit
- Sun-synchronicity
- A mean local sun time of 12:00 at the descending node
- Exact repeatability of position and velocity in the ECEF frame after one repeat cycle

In order to generate the reference trajectory that satisfies the above requirements, a nonlinear optimization problem is defined and solved with an iterative process. The basic concept and formulation used are similar to that presented by D'Amico [6]. Propagation is repeated with small changes in initial orbital elements until all of the requirements are achieved. The frozen orbit eccentricity is refined using Rosengren's algorithm [7] [6]. The obtained osculating orbit for a repeat cycle that comprises 207 orbital revolutions is the reference trajectory.

The generated reference trajectory data is the target of the autonomous orbit control. Therefore, it should be installed in the memory of the on-board flight computer and processed in real-time to compute current orbit errors. However, the generated reference trajectory, which is actually a large amount of data for the osculating ephemerides of a repeat cycle, e.g., 14 days and 207 revolutions for the ALOS-2 case, is not suitable for on-board installation. This is because the entire reference orbit's ephemerides set is superfluous; moreover, it requires a large amount of on-board memory resources. For this reason, only the essential reference orbit information required by the on-board orbit controller, such as the longitude and mean orbital elements at the descending node, are stored on-board. Accordingly, the orbital element vector for the orbital tube control $\boldsymbol{\alpha}$ is defined as follows:

$$\boldsymbol{\alpha}_j = \left(T_j, \bar{\boldsymbol{e}}_j^T, \bar{i}_j, \lambda_j\right)^T \tag{1}$$

where T_j is a nodal period defined as the duration between one crossing of a descending node and the next, $\bar{\boldsymbol{e}}_j$ is a mean eccentricity vector, $\bar{i}_j$ is the mean inclination, λ_j is the longitude of the descending node, and j is the pass number. The reference orbital element vector is noted as $\boldsymbol{\alpha}_{ref\,j}$ and the measured orbital element vector on the on-board flight computer is noted as $\boldsymbol{\alpha}_{meas\,j}$. A set of the reference orbital element vectors is generated on the ground for every orbital revolution of a repeat cycle. For the ALOS-2 case, the two hundred and seven reference orbital element vectors are prepared in total as the reference trajectory data for use on-board the satellite.

A nodal period T is used in this formulation instead of a mean semi-major axis $\bar{a}$, because it can be obtained directly and accurately on-board a satellite by measuring the interval between two successive descending node crossings. When geometrical interpretation is needed, an approximate value of the mean semi-major axis can be computed from the value of T by means of the following equation considering the J2 secular perturbation [8]:

$$T = \frac{2\pi}{n} \left\{ 1 - \frac{3J_2}{2} \left(\frac{R_e}{\bar{a}} \right)^2 \left(3 - 4\sin^2 \bar{i} \right) \right\} \tag{2}$$

where $n = \sqrt{\mu_e/\bar{a}^3}$, $J2$ is the second zonal gravity harmonic of the Earth, and R_e is the equatorial radius of the Earth.

3.3. Control Thresholds for the ALOS-2 Mission

The error of the current orbit with respect to the reference trajectory is obtained by subtracting the reference orbital element vector at each pass number from the measured orbital element vector as follows:

$$\Delta \boldsymbol{\alpha}_j = \boldsymbol{\alpha}_{meas\,j} - \boldsymbol{\alpha}_{ref\,j} \tag{3}$$

The purpose of the autonomous orbit control is to regulate the orbit error vector $\Delta\boldsymbol{\alpha}$ to within the specified control thresholds. As shown in Fig. 3, the orbit error for the orbital tube control is defined as the space error. Each element of $\Delta\boldsymbol{\alpha}$ contributes to the space error. The approximated mapping function between the orbit error vector $\Delta\boldsymbol{\alpha}$ and the space error $\boldsymbol{E}$ can be described as follows:

$$\boldsymbol{E} = \begin{pmatrix} E_N \\ E_R \end{pmatrix} = \begin{pmatrix} 0 & 0 & 0 & r\sin\bar{u} & r\sin(\bar{i}+\gamma)\cos\bar{u} \\ 1 & r\cos\bar{u} & r\sin\bar{u} & 0 & 0 \end{pmatrix} \begin{pmatrix} \Delta\bar{a} \\ \Delta\bar{e}_x \\ \Delta\bar{e}_y \\ \Delta\bar{i} \\ \Delta\lambda \end{pmatrix} \tag{4}$$

where γ is the angle between the inertial and Earth-fixed velocity vectors. Note that the mean semi-major axis error $\Delta\bar{a}$ is used in the above formulation instead of the nodal period error ΔT for

Table 2. Control Thresholds of the Orbit Error Vector for the ALOS-2 Mission

Parameter	3 σ dispersions	Comment
$\Delta\bar{a}$	100 m	equivalent to ΔT = 0.125 s
$\bar{a}\Delta\bar{e}_x$	150 m	
$\bar{a}\Delta\bar{e}_y$	150 m	
$\bar{a}\Delta\bar{i}$	367 m	0.003°
$\bar{a}\Delta\lambda$	367 m	0.003°

clear geometrical understanding. From this equation, it is understood that the control of the orbit error vector $\Delta\boldsymbol{\alpha}$ within the specified bounds leads directly to regulation of the space error $\boldsymbol{E}$.

The proper control thresholds for the orbit error vector $\Delta\boldsymbol{\alpha}$ can be assessed by Eq. 4. Each element of the orbit error vector $\Delta\boldsymbol{\alpha}$ is dealt with as a normally distributed stochastic variable, and the three sigma value, which corresponds to a space error of 500 m (3σ), is chosen as the control threshold. In Tab. 2 the computed control thresholds of $\Delta\boldsymbol{\alpha}$ are shown. The purpose of the autonomous orbit control is to regulate the $\Delta\boldsymbol{\alpha}$ within the control thresholds in the table to maintain the required accuracy of the orbital tube control.

4. Overview of the ALOS-2 Autonomous Orbit Control System

4.1. Architecture of the ALOS-2 Autonomous Orbit Control System

This section provides an outline of the proposed autonomous orbit control method, the architecture of which is shown in Fig. 4. The proposed method comprises five parts.

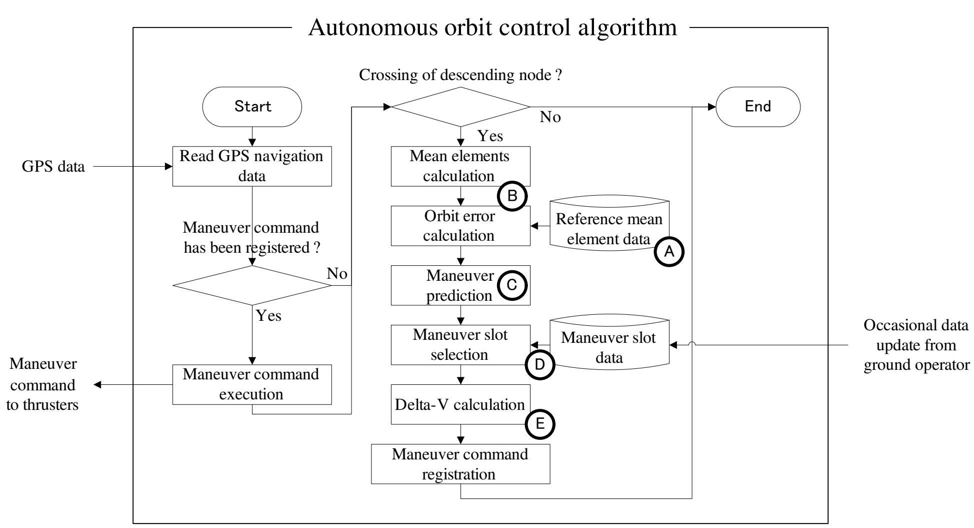

Figure 4. Architecture of the proposed autonomous orbit control method.

In the first part (“A” in Fig. 4), the Earth-fixed reference trajectory is generated and prepared. The reference trajectory data is transformed into the data set of the orbit error vector for each orbital revolution $\boldsymbol{\alpha}_r ef j$ and stored on an on-board computer.

The second part (“B” in Fig. 4) deals with on-board orbit determination and orbit error calculation. The on-board GPS navigation solutions are processed to determine the measured orbital element vector $\boldsymbol{\alpha}_m eas j$ precisely, and the orbit error vector $\Delta\boldsymbol{\alpha}_j$ with respect to the reference trajectory are calculated. In addition, a nodal period rate $\dot{T}$ is estimated by processing historical nodal period data.

In the third part (“C” in Fig. 4), precision maneuver prediction is performed. The equation describing the relationship between the longitude of descending node error $\Delta\lambda$ and the nodal period error ΔT, and the estimated nodal period rate $\dot{T}$, are utilized to predict the time of the next in-plane maneuver. The rigorous equation of the mean inclination variation which considers complex perturbations due to the gravity of Sun and Moon is used for the timing prediction of out-of-plane maneuver.

In the fourth part (“D” in Fig. 4), the idea of allocating a maneuver slot to avoid timing conflicts between automatically planned maneuvers and pre-planned payload data-take opportunities is applied. The maneuver slot data is uploaded in advance by ground operators. The autonomous on-board algorithm searches for and selects a preferable maneuver slot, which allows the on-board algorithm to decide on the maneuver execution time autonomously without concerns over the conflicts.

In the fifth part (“E” in Fig. 4),the on-board in-plane and out-of-plane Delta-V calculations are conducted. The algorithm predicts future trends in errors and determines proper velocity increments considering reduction of fuel, frequency of maneuvers and opportunities for deceleration maneuvers.

These five parts are integrated into the proposed autonomous orbit control method.

4.2. In-plane control concept

The autonomous orbit control system has to maintain the orbit control vector $\Delta\boldsymbol{\alpha}$ within the specified thresholds by velocity increments induced from impulsive maneuvers. The relationship between the velocity increments Δv_R, Δv_T, and Δv_N and desired relative orbit corrections can be described by the simplified Gauss equations adopted to near-circular nonequatorial orbits [9][10].

$$\begin{pmatrix} \Delta\bar{a} \\ \Delta\bar{e}_x \\ \Delta\bar{e}_y \\ \Delta\bar{i} \end{pmatrix} = \frac{1}{v} \begin{pmatrix} 0 & 2\bar{a} & 0 \\ \sin\bar{u} & 2\cos\bar{u} & 0 \\ -\cos\bar{u} & 2\sin\bar{u} & 0 \\ 0 & 0 & \cos\bar{u} \end{pmatrix} \begin{pmatrix} \Delta v_R \\ \Delta v_T \\ \Delta v_N \end{pmatrix} \tag{5}$$

The velocity increment in tangential direction: Δv_T leads to change of the mean semi-major axis $\bar{a}$ and the mean eccentricity vector $\bar{\boldsymbol{e}} = (\bar{e}_x, \bar{e}_y)^T$. Even the velocity increment in radial direction: Δv_R also causes change of the mean eccentricity vector, the radial maneuver is not used for the orbit control, because the efficiency of a maneuver in radial direction (Δv_R) to correct the eccentricity vector is half that of a correction made in tangential direction (Δv_T). Therefore, only the tangential maneuver is considered for the in-plane maneuvers.

It can be seen from Eq. 5 that in-plane and out-of-plane maneuvers are decoupled each other, resulting in independent control strategies of them. Therefore, the mean inclination $\bar{i}$ is controlled by a maneuver in normal direction (Δv_N) independently.

The variation in the longitude at the descending nodes considering only the J2 geopotential harmonic coefficient can be described as [8],

$$\Delta\lambda = \lambda - \lambda_0 = k_1(t-t_0) + \frac{1}{2}k_2(t-t_0)^2 \tag{6}$$

$$k_1 = \frac{1}{T}\left(\frac{\partial\lambda}{\partial\bar{a}}\Delta\bar{a}_0 + \frac{\partial\lambda}{\partial\bar{i}}\Delta\bar{i}_0\right) \tag{7}$$

$$k_2 = \frac{1}{T}\left(\frac{\partial\lambda}{\partial\bar{a}}\frac{d\bar{a}}{dt} + \frac{\partial\lambda}{\partial\bar{i}}\frac{d\bar{i}}{dt}\right) \tag{8}$$

where $\Delta\lambda$ is the ground-track drift from the initial value λ_0 where the last maneuver is performed, over the time interval $t-t_0$. Assuming the orbital decay rate $\frac{d\bar{a}}{dt}$ is constant for the interval, the evolution of the mean semi-major axis error $\Delta\bar{a}$ is modeled as:

$$\Delta\bar{a} = \Delta\bar{a}_0 + \frac{d\bar{a}}{dt}(t-t_0) \tag{9}$$

From substitution of Eq. 9 into Eq. 8, the parabolic drift profile of the longitude error $\Delta\lambda$ with respect to the semi-major axis error $\Delta\bar{a}$ is found. The control of the longitude error is achieved using this characteristic of the longitude error drift profile. The basic concept of the longitude control by in-plane maneuvers is shown in Fig. 5.

An in-plane maneuver is planned and executed at the close point near to the eastern limit of the longitude so that a semi-major axis error is raises from a negative value to a positive value to begin the drift of the longitude to the west. Afterwards the longitude of the ascending node drifts along the parabolic line on the $\Delta\lambda - \Delta\bar{a}$ plot. When the semi-major axis error decreases to zero, meaning it reaches to the reference altitude, the drift to the west stops and the point arrives at the summit of the parabolic line. Then it turns back to the east as the semi-major axis decreases to be negative. Subsequently, at the close point near to the eastern limit of the longitude, an in-plane maneuver is again executed. This sequence is repeated to regulate the longitude error within the specified tolerances by in-plane maneuvers.

When an in-plane maneuver which raises a semi-major axis is planned, an argument of latitude for

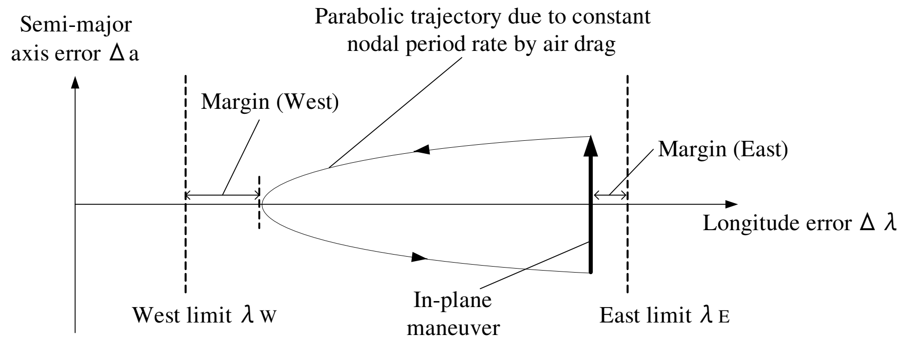

Figure 5. Concept of longitude control by in-plane maneuver.

execution of the maneuver is carefully selected to regulate an eccentricity vector error at the same time. The proper argument of latitude for an in-plane maneuver u_I is computed as [9],

$$u_I = \tan^{-1}\frac{\Delta\bar{e}_y}{\Delta\bar{e}_x} \tag{10}$$

As a result, it can be understood that four elements of the orbit error vector ($\Delta\bar{a}$, $\Delta\bar{e}_x$, $\Delta\bar{e}_y$, and $\Delta\lambda$) can be controlled by in-plane maneuvers.

4.3. Out-of-plane control concept

The only remaining element of the orbit error vector $\Delta\boldsymbol{\alpha}$ to be controlled by out-of-plane maneuvers is the inclination error $\Delta\bar{i}$. It can be seen from Eq. 5 that the inclination correction by velocity increments in normal direction (Δv_N) becomes the most efficient when it is executed at an ascending node ($u = 0°$) or a descending node ($u = 180°$). In case of ALOS-2 an ascending node is selected for the location of out-of-plane maneuvers.

To establish an efficient control strategy of the inclination, it is important to understand major perturbations which causes variation of it. The time derivative of inclination due to a perturbation described by a disturbing function R can be computed by the Lagrange planetary equation [8]:

$$\frac{di}{dt} = \frac{1}{na^2\sqrt{1-e^2}\sin i}\left(\cos i\frac{\partial R}{\partial \omega} - \frac{\partial R}{\partial \Omega}\right) \tag{11}$$

In case of the ALOS-2 orbit, the Sun and Moon third-body effects are the main cause of the variation. By applying the disturbing function of the third-body effect [11] to Eq. 11, the time derivative of inclination due to the third body effects is obtained. By integrating it over time, dropping trivial terms having a small amplitude, and arranging expressions, the variation of the mean inclination due to gravity of Sun for a near-circular sun-synchronous orbit can be described as:

$$\begin{aligned}\Delta\bar{i}_s &= \frac{3}{8}\frac{n_s}{n}\left\{C_{s0}n_s\Delta t - \sum_{k=1}^{2}\frac{C_{sk}}{k}\cos\left(kM_s+\alpha_{sk}\right)\right\} \\ &\equiv \Delta\bar{i}_{s0}+\Delta\bar{i}_{s1}+\Delta\bar{i}_{s2}\end{aligned} \tag{12}$$

and one due to gravity of Moon can be described as:

$$\begin{aligned}\Delta\bar{i}_m &= -\frac{3}{8}\frac{\mu_m}{\mu_m+\mu_e}\frac{n_m}{n}\left\{\sum_{k=1}^{2}\frac{C_{mk0}}{k\kappa_m}\cos k(\Omega-\Omega_m)+\frac{C_{m2-2}}{2\kappa_m-2}\cos\left(2\Omega-2\Omega_m-2M_m+\alpha_{m2-2}\right)\right\} \\ &\equiv \Delta\bar{i}_{m10}+\Delta\bar{i}_{m20}+\Delta\bar{i}_{m2-2}\end{aligned} \tag{13}$$

Detailed expressions of coefficients for Eq. 12 and 13 are summarized in Appendix A and B respectively. As seen in Eq. 12, there is a secular term $\Delta\bar{i}_S \equiv \Delta\bar{i}_{s0}$ by gravity of Sun, which is caused by the deep resonance due to sun-synchronicity. When an eccentricity of Sun is assumed to be small, the secular term can be approximated as [12] [13] :

$$\Delta\bar{i}_S = \Delta\bar{i}_{s0} = \frac{3}{8}\frac{n_s^2}{n}\sin i(1+\cos i_s)^2\sin\left(2L_s\right)\Delta t \tag{14}$$

As seen from this equation the extent is strongly dependent on the Mean Local Time (MLT) of the descending node L_s. If the MLT of a satellite orbit is close to 3:00, 9:00, 15:00, and 21:00, then the secular drift of the mean inclination is so rapid that the mean inclination increases or decreases monotonically. Conversely, if the MLT is close to 0:00, 6:00, 12:00, and 18:00 MLT, then the secular drift is so small that the periodic terms in Eq. 12 and 13 become dominant. Therefore the periodic terms are major contributors for variation of inclination for the ALOS-2 mission of which the MLT is 12:00.

The periodic terms in Eq. 12 and 13 can be divided into two categories. One is Long Period (LP) perturbations having one or half year periods ($\Delta\bar{i}_{s1}$, $\Delta\bar{i}_{s2}$, $\Delta\bar{i}_{m10}$ and $\Delta\bar{i}_{m20}$). The other is a Half Month (HM) perturbation ($\Delta\bar{i}_{m2-2}$). The overall variation of the mean inclination is sum of them and the secular term, which is small for the ALOS-2 case. Therefore, the variation of the mean inclination can be described as follows:

$$\Delta\bar{i} = \Delta\bar{i}_S+\Delta\bar{i}_{LP}+\Delta\bar{i}_{HM} \tag{15}$$

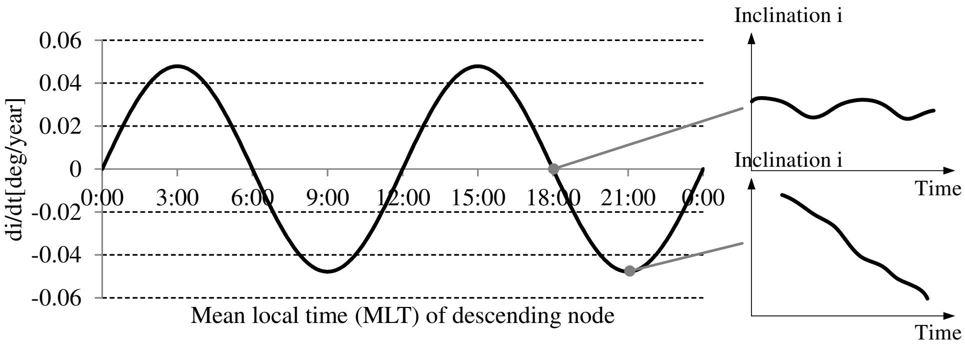

Figure 6. Secular perturbation of inclination due to gravity of Sun.

The computed annual variation of each term and structure of the variation of inclination for the ALOS-2 orbit are shown in Fig. 7. The maximum absolute variation of inclination due to the LP perturbation reaches up to 3×10^{-3} degrees, which corresponds to 367 m at the orbital altitude. The amplitude of the periodic inclination change due to the HM perturbation is 6×10^{-4} degrees, which corresponds to 73 m. The total variation of the mean inclination should be regulated within the control threshold specified in Tab. 2 under the perturbations consist of the LP and the HM terms.

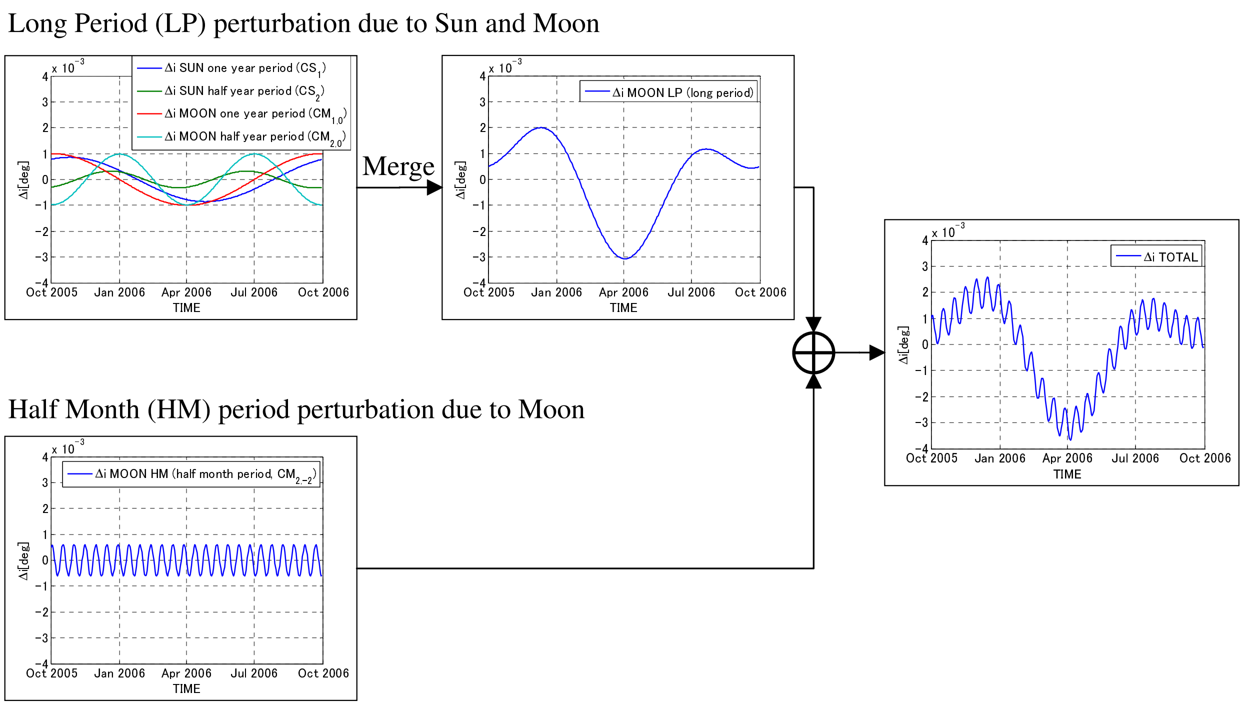

Figure 7. Structure of inclination perturbation for the 12:00 MLT ALOS-2 orbit.

Considering the above basic understandings of the variation of the mean inclination for the ALOS-2 orbit, a control strategy of out-of-plane maneuvers is designed. Figure 8 shows its concept. The target value to be controlled is the monthly averaged mean inclination $\Delta\bar{i}_{SL}$, which is obtained by subtracting $\Delta\bar{i}_{HM}$ from $\Delta\bar{i}$. The objective of the control is to regulate $\Delta\bar{i}_{SL}$ within $\pm\Delta\bar{i}_{th}$, which is a threshold value set to be 2×10^{-3} degrees (corresponds to 245 m) for the ALOS-2 case. Note that the sum of 245 m and 73 m, which is an amplitude of $\Delta\bar{i}_{HM}$ is less than the specified control threshold: 367 m. The on-board software can get the current mean inclination error $\Delta\bar{i}(t = t_0)$ from on-board GPS navigation solutions and obtain the current value of $\Delta\bar{i}_{SL}$ by subtracting $\Delta\bar{i}_{HM}$ from it. The future trend of $\Delta\bar{i}_{SL}$ can be computed as well by the on-board software using Eq. 12 and 13. When the predicted trend of $\Delta\bar{i}_{SL}$ exceeds the limit $\pm\Delta\bar{i}_{th}$ is the predicted time of the next out-of-plane maneuver. The proper velocity increments of the maneuver is computed so that the next coming extreme value of the $\Delta\bar{i}_{SL}$ trend, which is $\Delta\bar{i}_{lmin}$ or $\Delta\bar{i}_{lmax}$ in Fig. 8, coincides $-\Delta\bar{i}_{th}$ or $\Delta\bar{i}_{th}$ respectively. Actually the reason why $\Delta\bar{i}_{SL}$ instead of $\Delta\bar{i}$ is used as the control target is the ease of searching for the next maneuver timing by monitoring extreme values of its trend. Since the LP perturbation is the linear sum of trigonometrical functions as shown in Eq. 12 and 13, it is easy to design an on-board algorithm to find the next extreme value. As shown in Fig. 8, two out-of-plane maneuvers, one increases and the other decreases the mean inclination, are to be executed in a year.

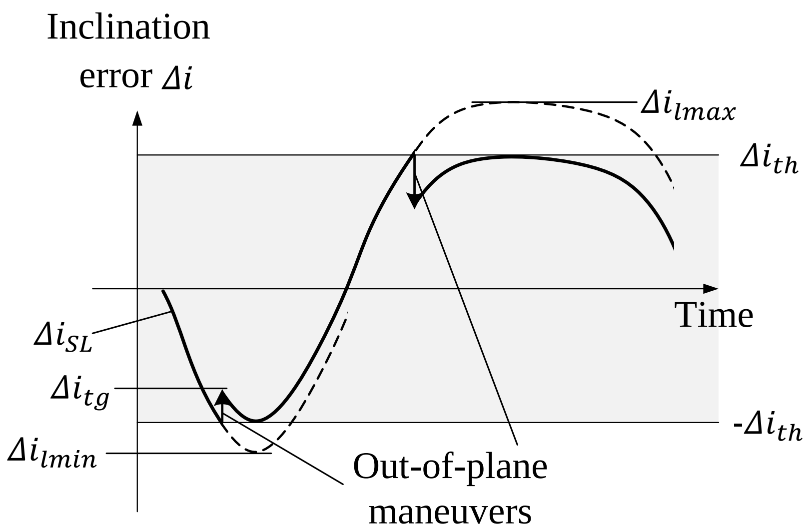

Figure 8. Concept of inclination control by out-of-plane maneuver.

4.4. Maneuver slot concept

Despite the autonomous orbit control representing a good solution to ease the workload, a new problem emerges: unexpected conflicts between mission observations and maneuver executions. The maneuver time should be planned to avoid payload data-take opportunities, thus guaranteeing the quality of observations. In general this coordination of time-sharing between maneuvers and observation operations has been realized by ground operators. Fully automatic decisions on maneuvers without consideration of mission observations can cause conflicts between them. To overcome this problem, the maneuver slot concept has been studied. The basic idea involves informing the on-board flight computer of planned observations in advance and allowing it to select the preferable maneuver time autonomously from known vacant periods when no other observation operations are planned. Figure 9 demonstrates the concept of the maneuver slot.

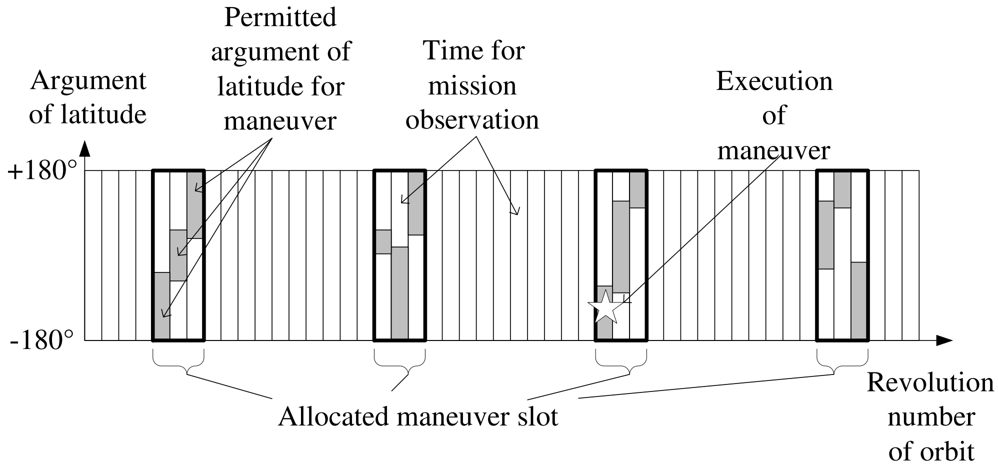

Figure 9. Concept of the maneuver slot.

The white area in Fig. 9 represents the periods used for mission observations, whereas the bold rectangles are the maneuver slots, containing hatched areas that accommodate the permitted argument of latitudes for orbital maneuvers. These maneuver slots are allocated by the ground operators and the data is sent to the on-board flight computer via telecommands.

In advance, ground operators establish an observation operation plan to cover the near future. The time span covered by the plan can be from one week to several months long. Subsequently, ground operators allocate maneuver slots in the timeline so that the permitted argument of latitude in a maneuver slot does not overlap with the payload data-take time. The number of allocated maneuver slots should exceed the predicted number of maneuvers to avoid any violation of orbit error requirements due to an unexpected rapid change in the orbital decay rate. For example, if the interval of in-plane maneuvers is predicted to be 10 days, the preferable interval for maneuver slots should be from 3 to 5 days. Note that the mission observation planning and the maneuver slot allocation are performed successively by a single mission planning system. The generated dataset of maneuver slots is sent to the on-board flight computer via telecommands.

The on-board flight computer compares the predicted time of its maneuver with the dataset of available maneuver slots, and subsequently, selects the farthest maneuver slot which does not exceed the predicted ideal maneuver timing t_I. The argument of latitude for the maneuver is selected so that the eccentricity vector error $\Delta\bar{\boldsymbol{e}}$ is properly regulated. Figure 10 shows how the maneuver slot is selected.

Based on the predicted ideal time of the next maneuver t_I, the dataset of available maneuver slots is searched backward and the slot just before t_I is selected. Subsequently, the argument of latitude is determined by the predicted error of the eccentricity vector $\Delta\bar{\boldsymbol{e}}$, meaning the revolution number and the exact time of the next maneuver are determined.

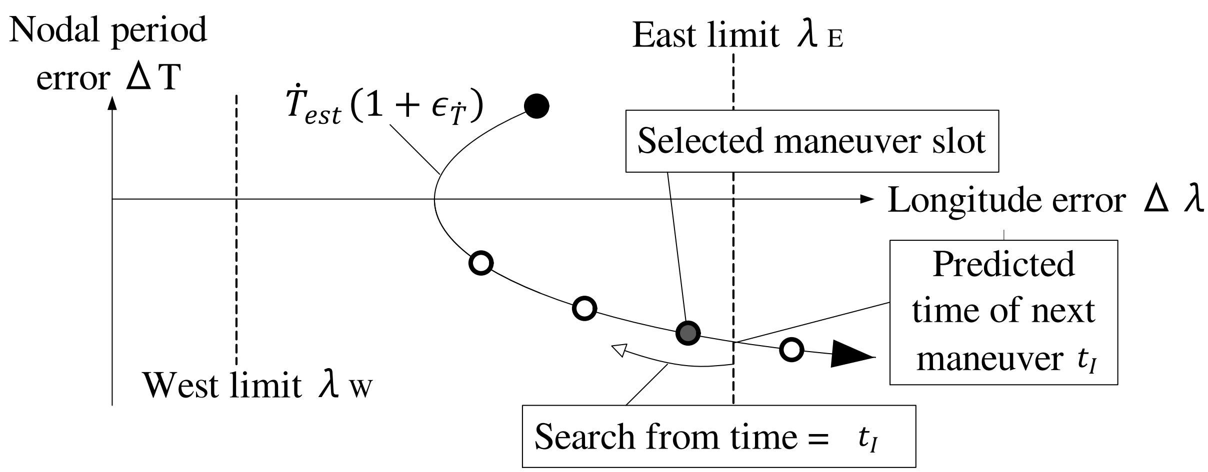

Figure 10. Selection of the maneuver slot.

5. ALOS-2 Flight Results of One-Year Operation

5.1. Initialization of Autonomous Orbit Control

The ALOS-2 was successfully launched on 24th May 2014 into the nominal 628-km sun-synchronous repeating orbit with a 14-day repeat cycle. The local sun time of the descending node is 12:00. As shown in 11, the launch date of the ALOS-2 was midway through the active period of an 11-year solar cycle. Therefore, ALOS-2 was expected to experience a significant orbital decay rate due to large atmospheric drag from the beginning of the operation.

Figure 11. F10.7 solar flux, averaged value over 81 days.

The autonomous orbit control function was initially disabled. Its functionalities were carefully validated step by step before its activation to ensure safety. The autonomy level for the ALOS-2 autonomous orbit control was selected for safety reasons. In Tab. 3, the definitions of the various levels are shown. The autonomy level was raised one level at a time from C to A as functional checks of the spacecraft were performed.

Table 3. Definition of autonomy level

Autonomy level	Orbit determination	Maneuver planning	Maneuver GO/NOGO
A	satellite	satellite	satellite
B	satellite	satellite	operator
C	operator	operator	operator

Initial corrections for launch injection errors and insertion into the reference orbit were performed at autonomy level C, which means that they were planned and commanded by ground operators according to conventional maneuver operation processes.

Subsequently, various functions of the autonomous orbit control, such as on-board GPS navigation, on-board orbit determination and error computation, on-board maneuver prediction, maneuver slot selection, and on-board Delta-V computation were confirmed as successful by analyzing telemetry data. Once the confirmation work was completely finished, the first maneuver by the ALOS-2 autonomous orbit control system was permitted on 28 July under autonomy level B, which means that the ground operators had to check the proposed maneuver plan in advance and then send a GO command to the spacecraft. When the autonomy level is B, the spacecraft does not perform the automatically planned maneuver without the GO command from the ground.

Once the result of the first maneuver had been evaluated and deemed successful, the autonomy level was raised to A in August. At this level, the spacecraft performs maneuvers without the GO command from the ground operators. Since then, the ALOS-2 autonomous orbit control system has been operated normally on a regular-basis at autonomy level A without any safety issues.

5.2. Autonomous In-Plane Orbit Control

Since the activation of the ALOS-2 autonomous orbit control system, both in-plane and out-of-plane maneuvers have been planned and performed autonomously up until the present time (Sep. 2015). In this section, the results of this in-plane orbit control are shown, and discussed.

Figure 12 shows the semi-major axis error $\Delta\bar{a}$ with respect to that of the reference trajectory. The control error has been regulated to within $\pm$ 40 m, which is smaller than the $\pm$100-m control thresholds, except for a short duration in March 2015. As described later, the debris avoidance maneuver was performed during this duration.

Figures 13 and 14 show the behaviors of the eccentricity vector error $\bar{a}\Delta\boldsymbol{e}$. The argument of latitude of the in-plane maneuvers is properly selected to control the error to within the 150-m control thresholds.

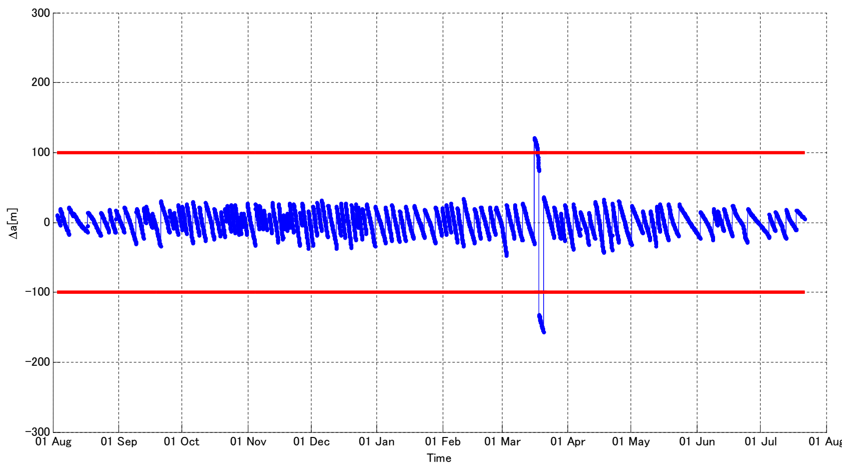

Figure 12. Semi-major axis error $\Delta\bar{a}$.

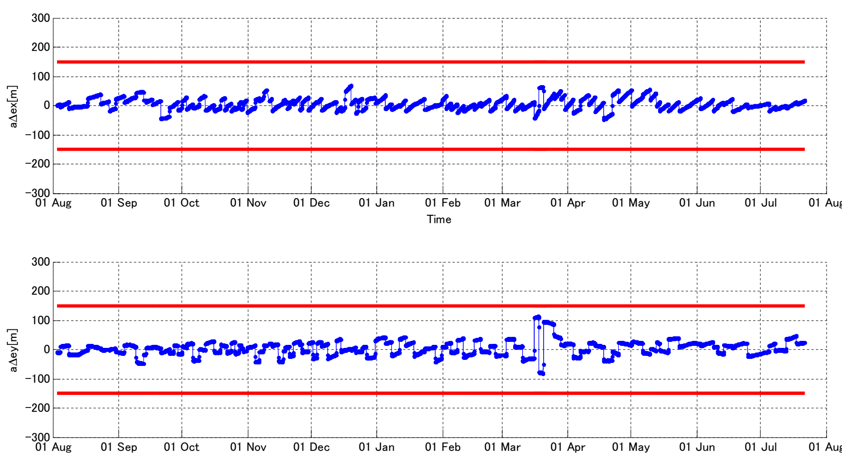

Figure 13. Eccentricity vector error $\Delta\bar{e}_x$ (top) and $\Delta\bar{e}_y$ (bottom).

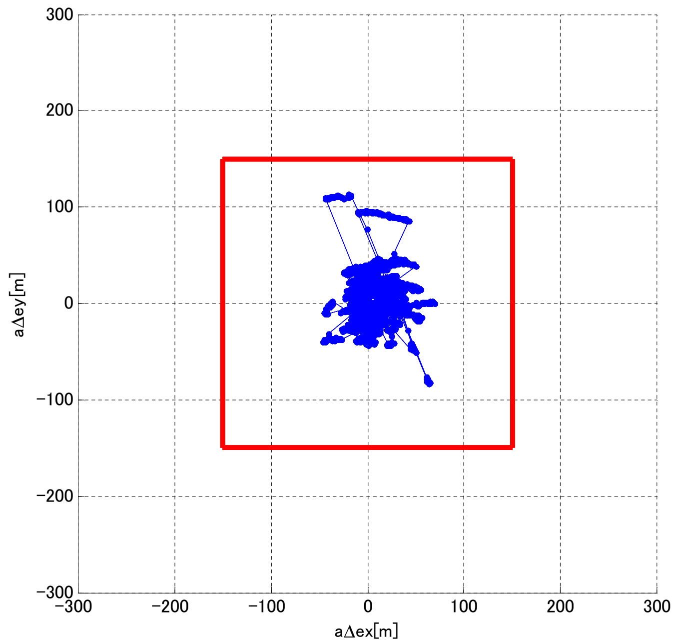

Figure 14. Eccentricity vector error, $\Delta\bar{e}_x - \Delta\bar{e}_y$ plot.

The longitude of the descending node error $\bar{a}\Delta\lambda$ with respect to the reference trajectory is shown in Fig. 15 and 16. During one year of operation, we have experienced two major opportunities of control threshold violation. One occurred in the middle of September 2014, which was shortly after the activation of the autonomous orbit control. The cause of the violation was found to be that some of the parameters in the on-board software were not set correctly. The parameters were promptly fixed, and a violation for this reason has not been repeated. The other incident occurred in the middle of March 2015. At that time, ALOS-2 performed a manual debris-avoidance maneuver. The daily in-plane maneuvers are performed autonomously, whereas conjunction analysis that looks for close approaches between any space objects and ALOS-2 is conducted by ground operators. When the probability of collision is considered to be higher than a specified threshold, a manual debris-avoidance maneuver is planned and commanded by ground operators. During the debris avoidance operation, the autonomous orbit control function is disabled temporarily. Except for the two incidents described previously, most of the control errors are regulated within the control thresholds.

Figure 17 shows the behavior of the longitude of the descending node error and the semi-major axis error before and after the debris avoidance maneuver. First, the autonomous orbit control function was disabled. Subsequently, the semi-major axis was raised through an acceleration maneuver to avoid the approaching space object. The longitude of the descending node then started to drift westward. Subsequently, a deceleration maneuver was performed to lower the semi-major axis so that the longitude of the descending node drifted back. Afterwards, the autonomous orbit control function was reactivated. The autonomously planned maneuver raised the semi-major axis properly so that the subsequent trajectory successfully returned to within the control thresholds. The whole debris avoidance operation took a week. We think that this duration was too long and should be improved. The duration between an acceleration maneuver and a deceleration maneuver should be shortened to reduce drifts of longitude. More efficient on-ground maneuver planning will be considered and tried during the next opportunity.

One of the lessons learned from the actual flight operation of the autonomous orbit control system is difficulty to dealt with a conjunction analysis operation. In recent years, many high value satellites perform conjunction analyses and, if necessary, to execute collision avoidance maneuvers. ALOS-2 chooses this policy as well. To ensure time for the conjunction analysis, the autonomous orbit control software of ALOS-2 has to decide the next maneuver plan and inform ground operators of it via telemetries priori to the planned maneuver execution time. Subsequently, ground operators make sure safety of the next maneuver by conjunction analyses. The minimum duration between the notification of the next maneuver plan and the actual maneuver execution is six revolutions. Due to the restriction caused by this necessity of conjunction analyses, the autonomous orbit control system has not been operated fully autonomously in a perfect sense even when the autonomy level is A.

Furthermore, the minimum maneuver interval is eventually limited due to the necessity of the notification to ground operators. Therefore, it should be noted that, when the autonomous orbit control approach is taken, a trade-off should be made between busyness of the conjunction analysis operation on ground and achievable accuracy of the orbit control by frequent orbital maneuvers.

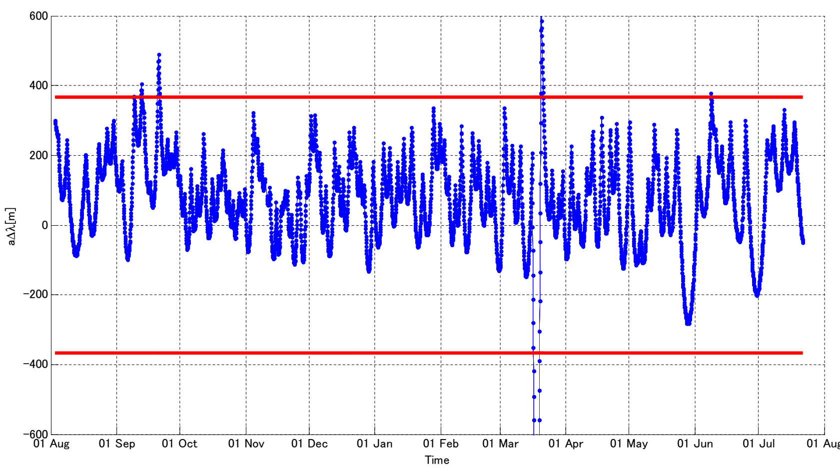

Figure 15. Longitude of descending node error $\bar{a}\Delta\lambda$.

The orbital decay rate, as estimated by the on-board software by utilizing GPS navigation, is shown in Fig. 18. As aforementioned the past year was in the middle of the most active period of an 11-year solar cycle. Therefore, the orbital decay rate was large and its variation was relatively extreme. Because the in-plane maneuvers are planned on the basis of the latest on-board estimation of the orbital decay rate, sometimes the on-board prediction of the longitude error become inaccurate due to a rapid jump in the orbital decay rate. This inaccuracy was actually assessed in advance so that the orbital decay prediction error was properly set as a parameter of the on-board software. Due

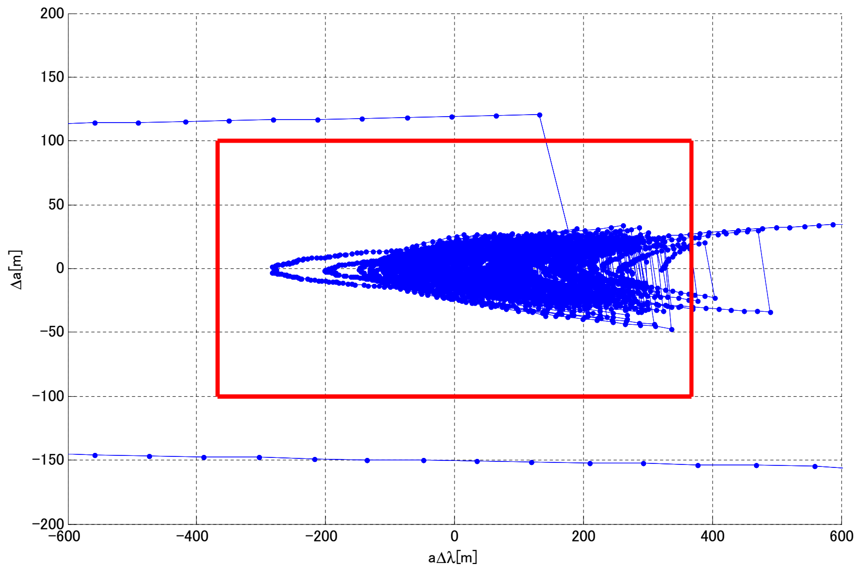

Figure 16. Longitude of descending node error ($\bar{a}\Delta\lambda$) - Semi-major axis error ($\Delta\bar{a}$).

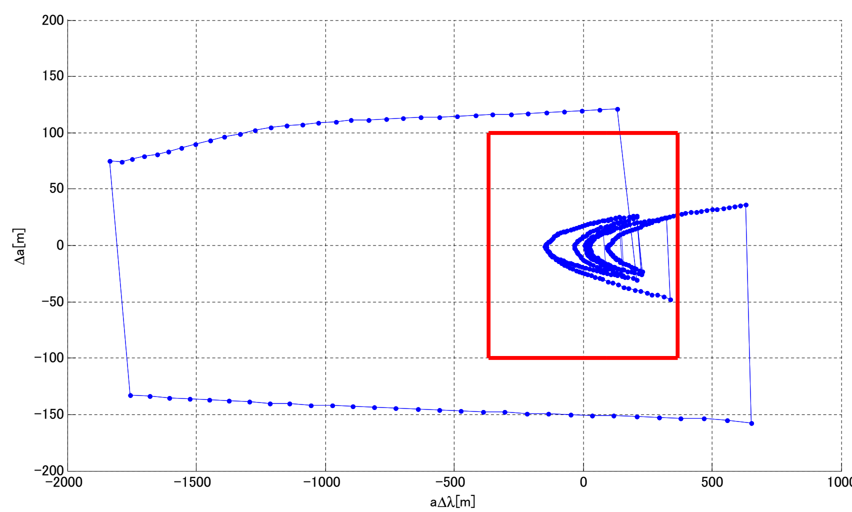

Figure 17. Longitude of descending node error ($\bar{a}\Delta\lambda$) - Semi-major axis error ($\Delta\bar{a}$) before and after the debris avoidance maneuver on March 2014.

to this, the longitude of the descending error has been regulated to within the control threshold as shown in Fig. 15, even during high levels of solar activity.

The proposed autonomous orbit control method simply uses the latest orbital decay rate, which is estimated by using real-time GPS navigation solutions, for prediction of the longitude error evolution in the future. From the results of the actual flight, the on-board prediction error of the orbital decay rate was found to be the greatest cause of the longitude control error. Even the strict tuning of the orbital decay prediction error could result in the accurate control of the longitude, it led to more or less inefficient frequent maneuver executions as well. Therefore, improvement of the orbital decay prediction should be effective to extend in-plane maneuver intervals. On-board atmospheric density computation using predicted space weather indices available on-line, which should be transmitted via commands to the satellite occasionally, may achieve better results. This approach will be investigated for future missions.

As seen in Fig. 11, the most intense solar period is now almost finished. From now on, the level of activity should decline gradually. Therefore the absolute value of the orbital decay rate will also gradually decrease in the future, and the frequency of in-plane maneuvers as well.

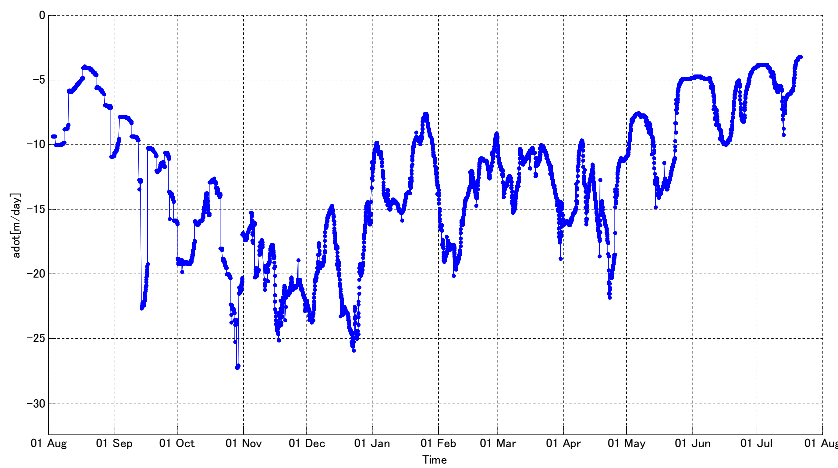

Figure 18. On-board orbital decay rate ($\dot{a}$) estimation results.

Figure 19 depicts in-plane maneuver activity from Aug. 2014-May. 2015, and a statistical summary is shown in Tab. 4. The in-plane maneuver Delta-V ranges from 1 to 4 cm/s. On Nov. 2014, as a conclusion of an investigation into the trend of the executed Delta-Vs and the longitude of the descending node, it was found that the control parameters were set too conservatively to avoid control threshold violation, which implies that too many small and frequent maneuvers were planned and executed. For this reason, we tried to find more appropriate control parameters and set them on 16th Nov. 2014. After this, both the Delta-V of the average maneuver and the interval between successive maneuvers increased as shown in Tab. 4. We have evaluated this parameter change as successful due to the larger Delta-V resulting in more efficient fuel usage and the longer maneuver intervals leading to efficient conjunction analysis operations, with these settings being enabled without violation of the control thresholds.

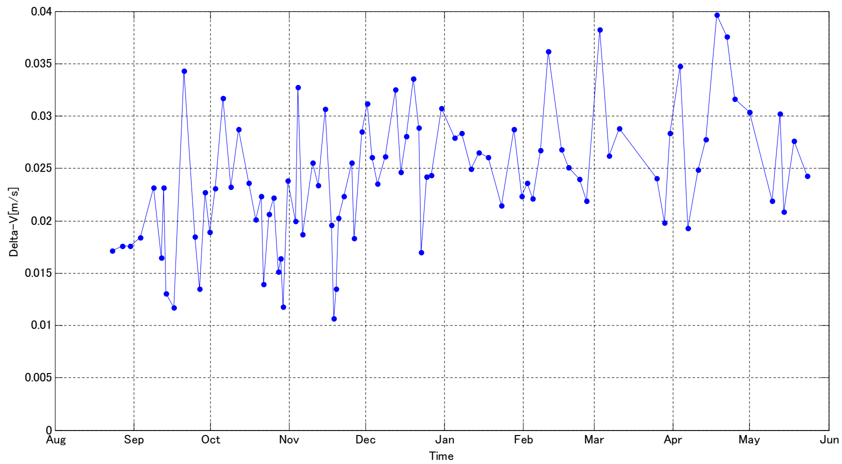

Figure 19. In-plane maneuver activity in Aug. 2014 - May. 2015.

Table 4. In-plane maneuver summary in Aug. 2014 to May. 2015.

	Before 16th Nov. 2014	After 16th Nov. 2014
Number of maneuvers	42	49
Average maneuver interval	2.4 days	3.8 days
Max. Delta-V	0.0343 m/s	0.0397 m/s
Ave. Delta-V	0.0208 m/s	0.0271 m/s
Min. Delta-V	0.0107 m/s	0.0170 m/s
Std. deviation of Delta-V	0.0058 m/s	0.0049 m/s

In Fig. 5 the number of used and allocated maneuver slots for each month are summarized. As the past year fell within the most solar active period, a maneuver slot was allocated for each day. It is expected that the density of maneuver slots will decrease (ex. a maneuver slot will be allocated every couple of days) in the future when the level of solar activity becomes much calmer. From Oct. to Nov. 2014, the orbital decay rate was so large that the maneuver slot use rate rose to 45 %. In contrast, from Jan. 2015 the use rate has been around 30 %. The causes of this change are believed to be the control parameter change on 16th Nov. 2014 and the decrease in the orbital decay rate. The positive correlation between the monthly averaged orbital decay rate and the maneuver slot use rate can be seen in Fig. 20. We will continue to monitor the monthly use rate to evaluate the density of the maneuver slot. If the use rate continues to be low for a substantial period, we will decrease the density of maneuver slots to make more room for payload data-take opportunities.

Table 5. Monthly record of used and allocated maneuver slots. (Duration for debris avoidance maneuver is excluded)

Month	Used slots	Allocated slots	Use rate [%]
Sep. 2014	11	30	36.7
Oct. 2014	14	31	45.2
Nov. 2014	14	30	46.7
Dec. 2014	13	31	41.9
Jan. 2015	8	31	25.8
Feb. 2015	8	28	28.6
Mar. 2015	8	28	28.6
Apr. 2015	7	30	23.3
May. 2015	6	29	20.7
Jun. 2015	6	30	20.0

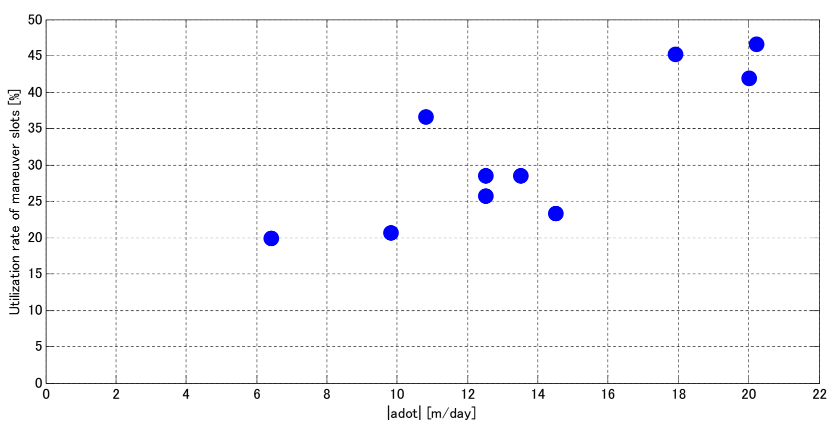

Figure 20. Monthly averaged orbital decay rate v.s. maneuver slot use rate.

5.3. Autonomous Out-Of-Plane Orbit Control

The MLT of the descending node of ALOS-2 is 12:00. Therefore, the secular perturbation of orbital inclination due to the gravity of the Sun is negligible. Instead, the half-monthly periodic perturbations due to the gravity of the Moon and Sun become dominant in terms of the inclination drift. Due to the small secular perturbation, the frequency of inclination maneuvers for the orbit with this MLT tends to be rather small. In the case of ALOS-2, two maneuvers per year are expected. The trend of the inclination error since activation of the autonomous orbit control is shown in Fig. 21 and a summary of the executed out-of-plane maneuvers is shown in Tab. 6. The first and the second out-of-plane maneuvers were performed successfully on 21st Jan. 2015 and 18th Jun. 2015, respectively. The averaged inclination $\bar{a}\Delta\bar{i}_{SL}$ is the value used as the control target by the on-board software. As shown in Fig. 6, the out-of-plane maneuver was computed so that the future extreme value of $\bar{a}\Delta\bar{i}_{SL}$ remained between the roughly 246 m ($2 \times 10^{-3} degrees$). The amplitude of the half-month period perturbation $\bar{a}\Delta\bar{i}_{HM}$ is about 73 m. Therefore the control error $\bar{a}\Delta\bar{i}$, which is the sum of $\bar{a}\Delta\bar{i}_{SL}$ and $\bar{a}\Delta\bar{i}_{HM}$, is expected to be within the $\pm$ 367-m control thresholds to make the spacecraft fly in the tube-shaped control window. The next out-of-plane maneuver will be performed on 26th Jan. 2015.

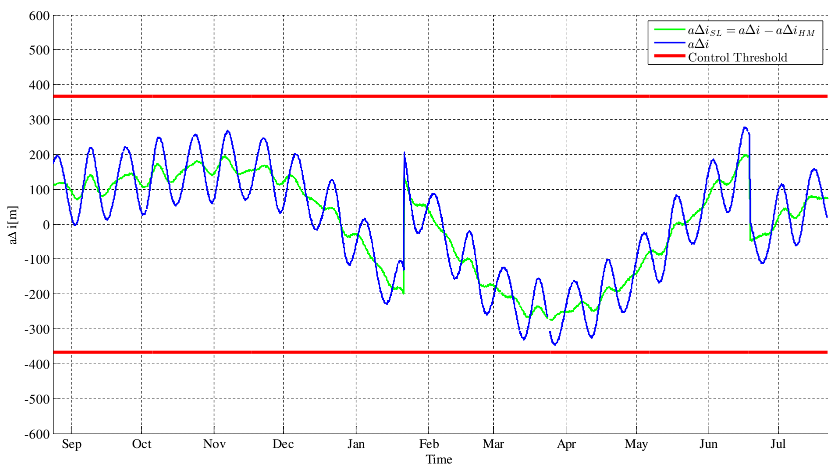

Figure 21. Inclination error $\bar{a}\Delta\bar{i}$.

Table 6. Out-of-plane maneuver record

	Date	Delta-V [m/s]
1st out of plane maneuver	21st Jan. 2015	0.358
2nd out of plane maneuver	18th Jun. 2015	-0.258

5.4. Orbital Tube Control Performance

The goal of the orbit control system is to make the spacecraft fly through the 500-m radius tube-shaped control window in an Earth-fixed frame with at least a 95 % success rate. To evaluate its performance, the actual trajectories obtained from on-board GPS navigation solutions are compared with the Earth-fixed reference trajectory. The entire one-year orbital trajectory from Aug. 2014 to Jul. 2015 is assessed at each evaluation plane, each separated by 30° of argument of latitude from the next, to evaluate the space error $\boldsymbol{E}$ defined in Fig. 3. A week spent on the debris-avoidance maneuver and recovery is excluded from the evaluation, because the autonomous orbit control function was disabled during that period. The total number of evaluation planes is 64961. Figure 22 shows the clearest result of the space error evaluation. A dot in the plot depicts the space error in normal and radial directions at an evaluation plane. As seen in the figure, most of the piercing points on the evaluation plane are inside the 500-m radius circle regardless of its arguments of latitude, except for rare violations in the normal direction. The computed probability of success is 99.7%, which far exceeds the required value of 95%. The RMS control errors are 151 and 59 m in the cross-track and radial directions, respectively.

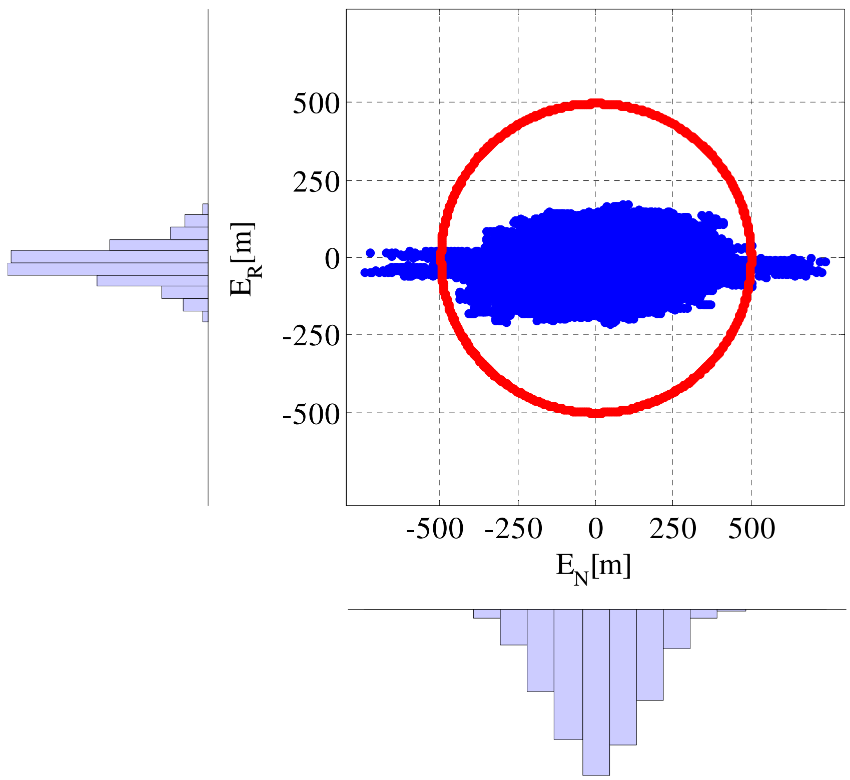

Figure 22. Space error and its statistical distribution.

Table 7. Orbital tube control performance

Evaluation period	From Aug. 2014 to Jul. 2015
Evaluation plane locations	Every 30° of argument of latitude
Number of evaluation planes	64961
Success probability of 500 m orbital tube control	99.7% (Requirement: 95%)
Space error in normal direction E_N (RMS)	151 m
Space error in radial direction E_R (RMS)	59 m

6. Conclusions

ALOS-2 was successfully launched on 24th May 2014. The orbit of ALOS-2 is a 628-km sun-synchronous repeating orbit with a 14-days repeat cycle. The orbit control requirement for the radius of the tube-shaped corridor is 500 m (95%).

The autonomous orbit control system has been demonstrated, and it has been in practical use since its activation in August 2014. This is the worlds first attempt to apply autonomous precision orbit control within a tube-shaped corridor for regular-basis operation of an Earth observation satellite.

The in-plane maneuvers were executed three times per week on average during the most active solar period. The automatic operation of such frequent in-plane maneuvers greatly helps with efficient ground operations of ALOS-2. The maneuver slot concept has been working well to prevent conflicts between mission observations and maneuver timing, and to achieve a flexible mission observation plan even when an autonomous maneuver planning approach is taken. The conjunction analysis operation was found to be one of the difficulties of the autonomous orbit control approach. When the approach is taken, a trade-off should be made between busyness of the conjunction analysis operation on ground and achievable accuracy of the orbit control by frequent orbital maneuvers. The out-of-plane maneuvers have also been performed autonomously.

The orbit control error with respect to the reference trajectory was evaluated. The majority of piercing points of the actual flight path are inside the required 500-m radius circle regardless of its argument of latitudes. The computed probability of success of the autonomous orbit control is 99.7%, and the probability of success is far more than the required 95%. This performance contributes to the good coherence between repeat-pass SAR image pairs of the ALOS-2 data products. The functionality and performance of the autonomous orbit control are planned to be monitored and evaluated continuously throughout the mission life of the ALOS-2. In particular, the behavior of in-plane maneuvers during the coming less active solar period will be carefully investigated.

The 500 m requirement of the ALOS-2 comes from its SAR design and differs depending on the SAR RF frequency, antenna size, and signal bandwidth. SAR systems with higher RF frequencies (such as C or X bands) tend to require far smaller corridor radii, such as 50-250 m, compared with the L-band ALOS-2 SAR system, which leads to more frequent in-plane maneuvers. In addition, the frequency of out-of-plane maneuvers dramatically changes depending on the MLT of the orbit. Accordingly, the orbit in some MLTs requires more frequent out-of-plane maneuvers than that of the ALOS-2. The proposed autonomous orbit control method is expected to be applicable to more stringent control constraints and more frequent out-of-plane maneuvers. A practical conjunction analysis operation method for the autonomous orbit control approach should be studied to realize it. The application of this proposed method to other Earth observation satellites with different requirements and MLTs will be investigated in the future.

A Coefficients to compute perturbations on inclination due to gravity of Sun

$$
\begin{aligned}
C_{s0} = &\left(\frac{1}{2} - \frac{5}{4}e_s^2\right)\sin i(1+\cos i_s)^2 \sin 2L_s \\
&+ \frac{1}{2}e_s \cos i \sin i_s \left\{6\cos i_s \sin\left(L_s+\omega_s\right) + (1+\cos i_s)\sin\left(L_s-\omega_s\right)\right\} \\
&+ \frac{9}{4}e_s^2 \sin i \sin^2 i_s \sin 2(L_s+\omega_s)
\end{aligned} \tag{16}
$$

$$
\begin{aligned}
C_{s1}\cos\alpha_{s1} = &\left(2 - \frac{3}{2}e_s^2\right)\cos i \sin i_s \cos i_s \cos\left(L_s+\omega_s\right) \\
&+ \frac{3}{2}e_s \sin i \sin^2 i_s \cos 2(L_s+\omega_s) \\
&+ \left(1 - \frac{5}{2}e_s^2\right)\cos i \sin i_s (1+\cos i_s)\cos\left(L_s-\omega_s\right) \\
&- 2e_s \sin i(1+\cos i_s)^2 \cos 2L_s
\end{aligned} \tag{17}
$$

$$
\begin{aligned}
C_{s1}\sin\alpha_{s1} = &\left(2 + \frac{15}{2}e_s^2\right)\cos i \sin i_s \cos i_s \sin\left(L_s+\omega_s\right) \\
&+ \frac{3}{2}e_s \sin i \sin^2 i_s \sin 2(L_s+\omega_s) \\
&- \left(1 - \frac{5}{2}e_s^2\right)\cos i \sin i_s (1+\cos i_s)\sin\left(L_s-\omega_s\right) \\
&+ \frac{3}{2}e_s \sin i(1+\cos i_s)^2 \sin 2L_s
\end{aligned} \tag{18}
$$

$$
\begin{aligned}
C_{s2}\cos\alpha_{s2} = &\left(1 + \frac{3}{2}e_s^2\right)\sin i \sin^2 i_s \cos 2(L_s+\omega_s) \\
&- \frac{17}{4}e_s^2 \sin i(1+\cos i_s)^2 \cos 2L_s \\
&+ \frac{1}{2}e_s \cos i \sin i_s \left\{\begin{aligned}&6\cos i_s \cos\left(L_s+\omega_s\right) \\ &-(1-\cos i_s)\cos\left(L_s+3\omega_s\right) \\ &+7(1+\cos i_s)\cos\left(L_s-\omega_s\right)\end{aligned}\right\}
\end{aligned} \tag{19}
$$

$$
\begin{aligned}
C_{s2}\sin\alpha_{s2} = &\left(1+\frac{3}{2}e_s^2\right)\sin i\sin^2 i_s\sin 2(L_s+\omega_s) \\
&+\frac{17}{4}e_s^2\sin i(1+\cos i_s)^2\sin 2L_s \\
&+\frac{1}{2}e_s\cos i\sin i_s\left\{\begin{array}{l} 6\cos i_s\sin(L_s+\omega_s) \\ -(1-\cos i_s)\sin(L_s+3\omega_s) \\ -7(1+\cos i_s)\sin(L_s-\omega_s) \end{array}\right\}
\end{aligned} \tag{20}
$$

$$
C_{sk} = \sqrt{(C_{sk}\cos\alpha_{sk})^2+(C_{sk}\sin\alpha_{sk})^2} \tag{21}
$$

$$
\alpha_{sk} = \tan^{-1}\frac{C_{sk}\sin\alpha_{sk}}{C_{sk}\cos\alpha_{sk}} \tag{22}
$$

B Coefficients to compute perturbations on inclination due to gravity of Moon

$$
C_{m10} = \left(1+\frac{3}{2}e_m^2\right)\cos i\sin 2i_m \tag{23}
$$

$$
C_{m20} = \left(1+\frac{3}{2}e_m^2\right)\sin i\sin^2 i_m \tag{24}
$$

$$
\begin{aligned}
C_{m2-2}\cos\alpha_{m2-2} = &\frac{9}{4}e_m^2\sin i\sin^2 i_m \\
&+\left(\frac{1}{2}-\frac{5}{4}e_m^2\right)\sin i(1+\cos i_m)^2\cos 2\omega_m
\end{aligned} \tag{25}
$$

$$
C_{m2-2}\sin\alpha_{m2-2} = -\left(\frac{1}{2}-\frac{5}{4}e_m^2\right)\sin i(1+\cos i_m)^2\sin 2\omega_m \tag{26}
$$

$$
C_{m2-2} = \sqrt{(C_{m2-2}\cos\alpha_{m2-2})^2+(C_{m2-2}\sin\alpha_{m2-2})^2} \tag{27}
$$

$$
\alpha_{m2-2} = \tan^{-1}\frac{C_{m2-2}\sin\alpha_{m2-2}}{C_{m2-2}\cos\alpha_{m2-2}} \tag{28}
$$

C References

[1] Suzuki, S., Kankaku, Y., and Osawa, Y. "ALOS-2 current status and operation plan." "SPIE Remote Sensing," pp. 888908–1–888908–11. International Society for Optics and Photonics, 2013.

[2] Krieger, G., Moreira, A., Fiedler, H., Hajnsek, I., Werner, M., Younis, M., and Zink, M. "TanDEM-X: A satellite formation for high-resolution SAR interferometry." Geoscience and Remote Sensing, IEEE Transactions on, Vol. 45, No. 11, pp. 3317–3341, 2007.

[3] Gens, R. and Van Genderen, J. "Review Article SAR interferometry - issues, techniques, applications." International Journal of Remote Sensing, Vol. 17, No. 10, pp. 1803–1835, 1996.

[4] Zebker, H., Villasenor, J., et al. "Decorrelation in interferometric radar echoes." Geoscience and Remote Sensing, IEEE Transactions on, Vol. 30, No. 5, pp. 950–959, 1992.

[5] Arbinger, C., D'Amico, S., and Eineder, M. "Precise ground-in-the-loop orbit control for low earth observation satellites." "18th International Symposium on Space Flight Dynamics," Vol. 548, p. 333. 2004.

[6] D'Amico, S., Arbinger, C., Kirschner, M., and Campagnola, S. "Generation of an optimum target trajectory for the TerraSAR-X repeat observation satellite." "18th International Symposium on Space Flight Dynamics," Vol. 548, p. 137. 2004.

[7] Rosengren, M. "Improved technique for passive eccentricity control." "Orbital Mechanics and Mission Design," Vol. 1, pp. 49–58. 1989.

[8] Vallado, D. A. Fundamentals of astrodynamics and applications. Springer, 2001.

[9] D'Amico, S. and Montenbruck, O. "Proximity operations of formation-flying spacecraft using an eccentricity/inclination vector separation." Journal of Guidance, Control, and Dynamics, Vol. 29, No. 3, pp. 554–563, 2006.

[10] Micheau, P. Orbit Control Techniques for Low Earth Orbiting (LEO)Satellites. Spaceflight Dynamics, Cepadues-Editions, edited by J. P. Carrou, Toulouse, France, 1995.

[11] Kozai, Y. "On the Effects of the Sun and the Moon upon the Motion of a Close Earth Satellite." SAO Special Report, Vol. 22, p. 2, 1959.

[12] Lee, B.-S. "Variations of the Local Time of Ascending Node for the Initial Inclinations of the KOMPSAT." Journal of Astronomy and Space Sciences, Vol. 16, No. 2, pp. 167–176, 1999.

[13] Chobotov, V. A. Orbital mechanics, third edition. AIAA Education Series, 2002.